Optimising the Operating Conditions of a New Robot Industrial Process Using Soft Computing Techniques

E. Corchado[1], J. Sedano[2], L. Curiel[3] and J.R. Villar[4]

[1] Department of Computer Science and Automatic Control, University of Salamanca, Salamanca, Spain

[2] Department of Electromechanical Engineering, University of Burgos, Burgos, Spain

[3] Department of Civil Engineering, University of Burgos, Burgos, Spain

[4] Department of Computer Science, University of Oviedo, Spain

This interdisciplinary research is based on the application of unsupervised connectionist architectures in conjunction with modelling systems and on the determining of the optimal operating conditions of a new industrial process known as laser milling. Laser milling is a relatively new micro-manufacturing technique in the production of high-value industrial components. The industrial problem is defined by a data set relayed through standard sensors situated on a laser-milling centre, which is a machine tool for manufacturing high-value micro-moulds, micro-dies and micro-tools. The new three-phase industrial system presented in this study is capable of identifying a model for the laser-milling process based on low-order models. The first two steps are based on the use of unsupervised connectionist models. The first step involves the analysis of the data sets that define each case study to identify if they are informative enough or if the experiments have to be performed again. In the second step, a feature selection phase is performed to determine the main variables to be processed in the third step. In this last step, the results of the study provide a model for a laser-milling procedure based on low-order models, such as Black Box, in order to approximate the optimal form of the laser-milling process. The

three-step model has been tested with real data obtained for three different materials: aluminium, cooper and hardened steel. These three materials are used in the manufacture of micro-moulds, micro-coolers and micro-dies, high-value tools for the medical and automotive industries among others. As the model inputs are standard data provided by the laser-milling centre, the industrial implementation of the model is immediate. Thus, this study demonstrates how an industrial process can be improved using a combination of artificial intelligence and identification techniques.

Keywords: Unsupervised Learning; Exploratory Projection Pursuit; Modelling Systems; Industrial Applications.

1. Introduction

Owing to the fast development of the manufacturing capabilities of countries such as China and India, traditional manufacturing is currently looking for new challenges. One such opportunity is in the manufacture of high-value micro-tools for different industrial sectors. Examples of these tools are those used in the field of medical therapeutics (odonto-stomatology) for bucco-dental rehabilitation and restoration in the processing and manufacturing of bucco-dental prosthesis, such as partial crowns, inlays and onlays, and partial and complete prosthesis fitted on structures of different metals, such as titanium, chrome cobalt, noble metals, etc., in which the optimising of the registering and mapping of the surgical field to be operated on is required. Other examples are steel moulds with deep marking for serial numbers or barcodes for quality control for the automotive industry, aluminium moulds with highly-complex 3D micro-shapes for medical applications or copper electrodes for electrical discharge machining (EDM). These tools are characterised by requiring critical 3D shapes or deep vertical walls somewhere on their surfaces. The generation of these geometries can be done using high-accuracy, high-speed milling or EDM, but both technologies have a physical limit where the 3D shapes are very small. A new technology is called for to surpass this limit: laser-milling (Ion, 2005).

Laser milling consists in the controlled evaporation of material caused by its interaction with a high-energy pulsed laser beam. The amount of vaporized material depends not only on laser pulse characteristics, but also on the composition of the material to be removed (Henry et al., 2004; Kuhl, 2002). A conventional milling machine knows in every moment the amount of material removed (the whole volume of the mill), but this is not so easy for a laser-milling centre. The usual proposal to solve this problem is the development of analytical or empirical models fit to the process behaviour (Harrison et al., 2004; Tani et al., 2008; Witte et al., 2008). However, these models always take those variables that perfectly fit the physical process as input data. Unfortunately, these variables can not be measured easily on real-world industrial machines that implement laser-milling technology. Therefore, to facilitate the quick take-up of this technology by industry, it is necessary to develop a model that can predict the exact amount of material that each laser pulse can get out using input data variables that can be obtained directly from real-world machines. This model will provide the control of laser milling with the accuracy required for micro-tools and, also, the optimization of their manufacture. In this interdisciplinary study, such a model is obtained using a combination of conventional and soft computing models. Soft computing is a collection or set of computational techniques in machine learning, such as artificial neural networks, fuzzy systems and swarm intelligence, which investigate, simulate and analyse very complex issues and phenomena.

Unsupervised learning is used initially, as a preliminary phase before the modelling system is established, to analyse the internal structure of the data sets. Consequently, it is worth knowing whether the data sets are relevant and informative enough. Exploratory projection pursuit (EPP) (Caló, 2007; Diaconis and Freedman, 1984) is a statistical method aimed at solving the difficult problem of identifying structures in high-dimensional data, providing an interesting view of the internal structure of the data set representing the problem to be analysed using higher-order statistics such as kurtosis, which is a measure of how pointed a distribution is.

In EPP, a relevant structure is usually defined with respect to the fact that most projections of high-dimensional data onto arbitrary lines through most multi-dimensional data give almost

Gaussian distributions (Diaconis and Freedman, 1984). Thus, interestingness is usually defined in terms of how far the distribution is from the Gaussian distribution.

These models are also used in a second step to carry out feature selection (Liu and Yu, 2005; Guyon and Eliseeff, 2003) to identify the main variables to be used in the third step. Several neural projection models based on EPP are applied in this study to carry out the first two steps of this soft computing model.

In complex, multidimensional domains, such as in industry, some data sets may hinder their own internal structures. Variables may contain false correlations which hinder the process of detecting the underlying causes of a data set. Furthermore, some features may be redundant since the information they add is contained in other features or variables. Extra features may increase computation time and can interfere in the accuracy of the clustering or classification process.

Feature selection (Liu and Yu, 2005; Guyon and Eliseeff, 2003) improves classification by searching for the subset of features that best classifies the training data and decreasing computation time.

Finally, the third and last phase is based on the use of classical identification techniques to obtain a model of the normal operating conditions.

Thus, unsupervised learning, and specifically EPP, is used in conjunction with classical identification techniques to obtain a model of the dynamics for a real-world industrial process—laser milling in this case. EPP is used to extract the relevant structures and relationships between variables to guarantee that the data set obtained by the sensors during the experiments is informative enough to identify the most significant features. The classical identification techniques then model the laser-milling conditions to choose the correct working parameters. Finally, the estimated working parameters facilitate increasing the quality of the resulting pieces.

This study presents the three-step procedure designed to identify the optimal conditions of a laser-milling process. The paper is organised as follows: Section 2 introduces the unsupervised connectionist techniques used for analysing the data to extract the relevant internal structures.

This is the first step in the modelling process. The second step, feature selection, is described in section 3, which serves to select the main variables to be processed in the third step. Section 4 describes the classical identification techniques used in the system modelling (third step). Section 5 provides details on the application field and the case studies and an analysis and comparison of the best models and results. Lastly, conclusions and future work are discussed.

2. Relevant Internal Structure Extraction Using Projection Methods

Principal component analysis (PCA) (Esbensen and Geladi, 2009), first found in Pearson's research (Pearson, 1901) and independently in Hotelling's (Hotelling, 1933), is a statistical method describing multivariate data set variations as uncorrelated variables, each of which is a linear combination of the original variables. Its main goal is to derive new variables in decreasing order of importance (variance), which are linear combinations of the original variables and are uncorrelated with each other. It is a well-known technique that can be implemented by a number of connectionist models (Fyfe, 1993; Oja, 1982). The PCA aims to find that orthogonal basis that maximises the data's variance for a given dimensionality of basis. The PCA is the most frequently reported linear operation involving unsupervised learning for data compression and feature selection.

The standard statistical method of EPP (Caló, 2007; Corchado et al., 2004; Friedman and Tukey, 1974) provides a linear projection of a data set. The data projections make use of a set of basis vectors that best reveals the relevant structures of the data. The relevancy is measured as interestingness, which is usually defined in terms of how far the distribution is from the Gaussian distribution (Seung et al., 1998).

One neural implementation of EPP is Maximum Likelihood Hebbian Learning (MLHL) (Corchado et al., 2004). MLHL has been widely used in the field of pattern recognition (Corchado et al., 2004; Corchado and Fyfe, 2003) as an extension of PCA. It identifies interestingness (Corchado et al., 2004; Friedman and Tukey, 1974) by maximising the

probability of the residuals under specific probability density functions that are non-Gaussian under the analysis of the fourth-order statistic, the kurtosis.

An extended version of this model is the Cooperative Maximum Likelihood Hebbian Learning (CMLHL) (Corchado and Fyfe, 2003). CMLHL is based on MLHL with the addition of lateral connections (Corchado and Fyfe, 2003) derived from the rectified Gaussian distribution (Seung et al., 1998). The resulting network can find the independent factors of a data set but it does so in a way that captures some type of global ordering in the data set.

Consider an N-dimensional input vector ($\boldsymbol{x}$), an M-dimensional output vector ($\boldsymbol{y}$) and a weight matrix $\boldsymbol{W}$, where the element $\boldsymbol{W_{ij}}$ represents the relationship between input x_j and output y_i. Then, as shown in (Corchado and Fyfe, 2003), the CMLHL can be carried out as a four steps procedure as follows:

Feed-forward step	$y_i = \sum_{j=1}^{\mathbf{N}} W_{ij} x_j, \forall i$	(1)
Lateral activation passing	$y_i(t+1) = \left[y_i(t) + \tau(b - Ay) \right]^+$	(2)
Feedback step	$e_j = x_j - \sum_{i=1}^{M} W_{ij} y_i, \ \forall j$	(3)
Weights changing step	$\Delta W_{ij} = \eta y_j sign(e_j) \lvert e_j \rvert^{p-1}$	(4)

Where: η is the learning rate, the rectification $[\ ]^+$ is necessary to ensure that the y -values remain within the positive quadrant; τ is the "strength" of the lateral connections, b the bias parameter and p is a parameter related to the energy function (Corchado et al., 2004; Corchado and Fyfe, 2003).

A is a symmetric matrix used to modify the response to the data whose effect is based on the relation between the distances among the output neurons. It is based on the cooperative distribution, but to speed learning up, it can be simplified to:

$$A(i,j) = \delta_{ij} - \cos\left(2\pi(i-j)/M\right) \tag{5}$$

Where δ_{ij} is the Kronecker delta and M is the number of outputs (Figure 1).

The A matrix is used to modify the response to the data based on the relation between the distances between the outputs. The outputs are thought of as located on a ring ("wraparound").

Figure 1. The A Matrix for the rectified Gaussian network with 24 outputs. Black squares are negative, white are positive and the shading in each square is proportional to the weight size.

The network's operation is the standard negative feedback operation with lateral connections. It is illustrated in Figure 2 (Eq. (1) to Eq. (4)).

Figure 2. Lateral connections between neighbouring outputs.

2.1. Lateral Connections

Lateral connections have been derived from the Rectified Gaussian distribution (Seung et al., 1998), which is a modified version of the standard Gaussian distribution in which the variables are constrained to be non-negative, enabling the use of non-convex energy functions. The standard Gaussian distribution may be defined by:

$$p(y) = Z^{-1} e^{-\beta E(y)} \tag{6}$$

$$E(y) = \frac{1}{2} y^T A y - b^T y \tag{7}$$

In which the quadratic energy function $E(y)$ is defined by the vector b and the symmetric matrix A. The parameter $\beta = 1/T$ is an inverse temperature. Lowering the temperature concentrates the distribution at the minimum of the energy function. The factor Z normalizes the integral of $p(y)$ to unity.

The cooperative distribution is chosen as its modes are closely spaced along a non-linear continuous manifold. The energy functions that can be used are those that block the directions in which the energy diverges towards negative infinity. Thus, the matrix has to fit the following property:

$$y^T A y > 0, \forall y : y_i > 0, i = 1 \ldots N \tag{8}$$

In which, N is the dimensionality of y.

The cooperative distribution in the case of N variables is defined by Eq. (9) and Eq. (10):

$$A_{ij} = \delta_{ij} + \frac{1}{N} - \frac{4}{N}\cos\left(\frac{2\pi}{N}(i-j)\right) \tag{9}$$

$$b_i = 1 \tag{10}$$

In which δ_{ij} is the Kronecker delta, and i and j, the output neuron identifiers.

Matrix A modifies the response to the data based on the relation between the distances between the outputs. The projected gradient method is used (Corchado et al., 2003), consisting of a gradient step followed by a rectification as specified in Eq. (2), in which the rectification $[\ ]^+$ is necessary to ensure that the y-values remain within the positive quadrant. If the step size (τ) is chosen correctly, this algorithm will probably be shown to converge to a stationary point of the energy function (Bertsekas, 1999). In practice, this stationary point is generally a local minimum.

The distribution mode can be approached by gradient descent on the derivative of the energy function Eq. (11) with respect to y:

$$\Delta y \propto -\frac{\partial E}{\partial y} = -(Ay - b) = b - Ay \tag{11}$$

The resulting model (CMLHL) can reveal the independent factors of a data set in a way that captures some type of global ordering in the data set and displays it with greater sparsity than other models.

Several versions of this model have successfully been applied to different data sets. Some of them are artificial, such as the well-known bars data set (Corchado and Fyfe, 2003; Földiák, 1992) while others are real, such as data sets on banking, asteroids, algae (Corchado and Fyfe, 2003) and knowledge management (Herrero et al., 2010).

2.2. Fine Tuning

The CMLHL fine-tuning process is based on the effect of changing the τ parameter, which is the strength of the lateral connections between the output neurons. Experiments were conducted

(Corchado and Fyfe, 2003) using the bars data set (Földiák, 1992), which adds noise in a graduated manner across the outputs. These experiments showed that altering the strength of the lateral connection parameter modulated the ability of the neural network to "gather" features together on the outputs. As predicted, a low τ value allows the neural model to code horizontal and vertical bars around a mode. An increase in the τ value means that the weak correlations between horizontal and vertical bars begin to have an impact on the learning. As the strength of the lateral connections becomes stronger, the bars are still learned around a mode but at the same time orientations start to separate. Subsequently, a separation emerges between the two different orientations, which is an interesting issue since all the data inputs to the network consist of both horizontal and vertical bars.

Increasing the τ value further will force the network to learn only one orientation of bars. However, if the lateral connections are too strong, then the coding of the bars may be squashed into an area of the output space that is too small for all of the bars to be coded individually. The reason why one orientation of bars is suppressed is due to the pixel overlap between different orientations of bars. If the lateral excitation between the output neurons is strong enough, a single output neuron may be able to switch its preference from a horizontal bar to a vertical one. That orientation identification was considered (Corchado and Fyfe, 2003) to be a precursor of the creation of the concept of horizontal/vertical in animals inhabiting a mixed environment.

3. Feature Selection and Extraction

Feature selection and extraction (Guyon and Eliseeff, 2003; Liu and Yu, 2005) includes feature construction (Gravilis et al., 2008), space dimensionality reduction (Liu et al., 2009b), sparse representations (Wright et al., 2009) and feature selection (Liu et al., 2009a). All these techniques are commonly used as pre-processing tools to machine learning tasks including pattern recognition. Although such problems have been tackled by researchers for many years, there has recently been a renewed interest in feature extraction. A large number of new applications with very large input spaces need space dimensionality reduction critically for the

efficiency and efficacy of the predictors. Some of these applications include new and classical topics such as bioinformatics (DNA microarrays (Gonzalez et al., 2009; Kim and Cho, 2006), remote sensing multi- and hyperspectral imagery (Malpica et al., 2008), pattern recognition (e.g., handwriting recognition (Su et al., 2009), text processing (Valeriana-Garcia et al., 2008), Web mining (Chen et al., 2009), speech processing (Avci, 2007; Mostafa and Billor, 2009), artificial vision (Raducanu et al., 2009), medical applications (Marinakis et al., 2009; Wolczowski and Kurzynski, 2010), industrial applications (Avci, 2009)).

The approach taken to feature selection is based on space dimensionality reduction. It initially uses a projection method called Cooperative Maximum Likelihood Hebbian Learning (CMLHL) (Corchado and Fyfe, 2003), which is characterized by its capability to enforce a sparser representation in each weight vector than other classical methods, such as PCA or Maximum Likelihood Hebbian Learning (MLHL).

The internal structures of complex clustering domains, such as high dimensional ones, may hinder their own internal structures or patterns. Such patterns may become visible if a change of basis of the space is made, however an a priori decision as to which basis will reveal most patterns requires foreknowledge of the unknown patterns.

CMLHL is an EPP model aimed at solving the previous difficult problem of identifying structure in high-dimensional data by projecting the data onto a low-dimensional subspace in which its structure is searched for by eye. However, not all projections will reveal the data's structure equally well. Therefore, an index has been defined that measures how “interesting” a given projection is; the data is represented in terms of projections that maximise that index. Interesting structure is usually defined with respect to the fact that most projections of high-dimensional data onto arbitrary lines through most multi-dimensional data give almost Gaussian distributions (Diaconis and Freedman, 1984). Therefore, to identify “interesting” features in data, directions should be looked for onto which the data-projections are as far from the Gaussian as possible. CMLHL is based on the analysis of the kurtosis, which is based on the normalised fourth moment of the distribution and measures the heaviness of the tails of a

distribution. A bimodal distribution will often have a negative kurtosis, meaning negative kurtosis can signal that a particular distribution shows evidence of clustering.

4. System Modelling Using Classical Identification Algorithms

4.1. Identification Criterion

The identification criterion consists in evaluating which of the group of candidate models is the best adapted and the one that best described the data set gathered for the experiment, i.e., given a certain model $M(\theta_*)$, its prediction error may be defined by Eq. (12). As stated in (Ljung, 1999), "a good model is one that makes good predictions, and which produces small errors when the observed data is applied". The estimated parametrical vector $\hat{\theta}_N$ is obtained in such a way that the prediction error $\varepsilon(t,\theta)$ is minimised for data set Z^t.

$$\varepsilon(t,\theta_*) = y(t) - \hat{y}(t \mid \theta_*) \tag{12}$$

So, minimising the error function $V_N(\theta, Z^N)$ generates the estimated parametrical vector $\hat{\theta}$. Typically, $V_N(\theta, Z^N)$ is calculated by the least-squares criterion for the linear regression, i.e., by applying the quadratic norm $\ell(\varepsilon) = \frac{1}{2}\varepsilon^2$, Eq. (13).

$$V_N(\theta, Z^N) = \frac{1}{N}\sum_{t=1}^{N}\frac{1}{2}(y(t) - \hat{y}(t \mid \theta))^2 \tag{13}$$

$$\hat{\theta} = \hat{\theta}_N(Z^N) = \arg\min_{\theta \in D_M} V_N(\theta, Z^N) \tag{14}$$

One of the available methodologies of model structure is the black-box structures (Ljung, 1999), which has the advantage of only requiring very few explicit assumptions on the pattern to be identified, but that in turn makes it difficult to quantify the model that is obtained. The discrete linear models may be represented through the union of both deterministic and stochastic models,

Eq. (15). In Eq. (15), *u(t)* is the input, *y(t)* is the output, $G(q^{-1})$ is the transfer function from *u(t)* to *y(t)*, $H(q^{-1})$ is the transfer function from *e(t)* to *y(t)* and q, q^{-1} are forward and backward shift operators. The term *e(t)* (white noise signal) includes the modelling errors and is associated with a series of random variables of mean null value and variance λ.

$$y(t) = G(q^{-1})u(t) + H(q^{-1})e(t) \tag{15}$$

The structure of a black-box model depends on how the noise influences the model (Ljung, 1999), that is, the term $H(q^{-1})$. Thus, if this term is 1, then the FIR (Finite Impulse Response) (Fernandes et al., 2010) and OE (Output Error) (Gillberg and Ljung, 2010; Taghavi and Sadr, 2008) models are applicable; whereas if it is different from zero a great range of models are applicable; the most common being: ARX (autoregressive with external input) (da Silva et al., 2009; Ismail et al., 2009), ARMAX (autoregressive moving Average with external input) (Iqbal et al., 2010; Wang and Cheng, 2009), BJ (Box Jenkins) (Meiler et al., 2008; Mustafaraj et al., 2010) and ARMA (autoregressive moving Average) (Datong et al., 2009; Huang et al., 2009). This structure may be represented in the form of a general model Eq. (16) and Eq. (18), where $B(q^{-1})$ is a polynomial of degree n_b, which can incorporate pure delay n_k in the inputs, and $A(q^{-1})$, $C(q^{-1})$, $D(q^{-1})$ and $F(q^{-1})$ are autoregressive polynomials of degree n_a, n_c, n_d and n_f, respectively. In the same way, it is possible to use a predictor expression, for the one-step prediction ahead of the output $\hat{y}(t \mid \theta)$, Eq. (17). The value of n_a, n_b, n_c, n_d, n_f and n_k are parameterized.

$$A(q^{-1})y(t) = q^{-n_k}\frac{B(q^{-1})}{F(q^{-1})}u(t) + \frac{C(q^{-1})}{D(q^{-1})}e(t) \tag{16}$$

$$\hat{y}(t \mid \theta) = \frac{D(q^{-1})B(q^{-1})}{C(q^{-1})F(q^{-1})}u(t) + \left[1 - \frac{D(q^{-1})A(q^{-1})}{C(q^{-1})}\right]y(t) \tag{17}$$

$$\begin{gathered} A(q^{-1}) = \sum_{i=1}^{n_a} 1 + a_i(q^{-1}), \quad B(q^{-1}) = \sum_{i=1}^{n_b} b_i(q^{-i}), \quad C(q^{-1}) = \sum_{i=1}^{n_c} 1 + c_i(q^{-1}), \\ D(q^{-1}) = \sum_{i=1}^{n_d} 1 + d_i(q^{-1}), \quad F(q^{-1}) = \sum_{i=1}^{n_f} 1 + f_i(q^{-1}) \end{gathered} \tag{18}$$

4.2. Modelling the Laser-Milling Optimal Conditions

This study tries to find the best model for estimating the optimal conditions of the laser-milling process. An identification procedure should be used so the experimentation can be carried out for different cases. As stated in (Haber and Keviczky, 1999a; Haber and Keviczky, 1999b; Ljung, 1999; Nelles, 2001; Nörgaard et al., 2000), the identification procedure includes establishing the identification techniques, the selection of the model structure, the estimation of the suitable polynomials degree, choosing the identification criterion and the optimization techniques to generate the final model.

Also, the identification procedure includes the training and the validation stages, which ensures that the selected model meets the necessary conditions for estimation and prediction. In order to validate the model, three tests were performed: the residual analysis $\varepsilon(t,\hat{\theta}(t))$ by means of a correlation test between inputs, the final prediction error (FPE) estimate as explained by Akaike (Akaike, 1969) and lastly the graphical comparison between desired outputs and the outcome of the models through simulation one (or k) steps before.

5. An Industrial Case Study: Choosing the Optimal Operating Conditions

In this study, a procedure to determine the optimal operating conditions for a laser-milling process is described. The procedure includes three steps, as shown in Figure 3. After data set gathering, in the first step, an analysis of the data set is performed to identify if it is informative enough. If the gathered data set is not valid, then it should be discarded and a new data set should be considered. The second step is based on feature selection to identify the most relevant variables; its outcome is the dimensional reduced data set. Finally, the third step involves searching for the model that best suits fits the operating conditions; its outcome is the model to be used, finding the best operating conditions in each case.

Figure 3. The flow chart of the proposed procedure.

The procedure is validated against three, common, real-world laser-milling problems in the industry. The first one is copper, a material used in the manufacture of electrodes for EDM. The second one is aluminium, a material commonly used for highly-complex moulds for medical applications. The third one is hardened steel, which is often used in the automotive industry, where laser milling allows the deep marking of serial numbers or barcodes for quality control. These three materials cover a broad range of industrial applications of laser milling and micro-manufacturing.

Modelling the laser-milling process involves several steps. After a data set is collected through the use of sensors, an internal structure analysis is carried out. The most significant variables then have to be identified. Finally, the model must be generated considering the most important variables and the relationships found. These steps are detailed below.

5.1. Data Set Generation

To describe the industrial problem, a test piece has been designed. The test piece is an inverted truncated pyramid profile that is to be laser milled on a flat metallic piece of the three selected materials. The truncated pyramid angles are theoretically of 135º and the depth (or height) of the truncated pyramid is 1 mm, but as the laser parameters are not known for these materials, both parameters will show an error on the real machined pieces called angle error and depth error, referred in this paper as y_1 and y_2, respectively. The prediction of the geometrical error through these two variables is enough to assure the geometrical quality of the micro-tools that will be machined by laser manufacturing.

The test piece was laser milled using a laser with a pulse length of 10μs. Some parameters of the laser process can be controlled: the laser power (u_1), the laser milling speed (u_2), the laser spot diameter, the distance from the laser focus to the piece (positioning along the Z-axis adjustment), the machining strategy and the laser pulse frequency (u_3). It is important to note that all these parameters are standard data provided by the laser-milling centre, so the industrial

implementation of the model will be immediate. For the data analysis, three other variables related to the milled material were also considered: thermal conductivity, reflectivity and density.

The experiment design included variation of all the parameters mentioned above, with the exception of laser spot diameter and machining strategy, which were constant for all tests. Almost 100 different experiments were carried out, which meant a large increase in the cost of the study. After the laser milling of the test piece previously described, the actual inverted pyramid depth and the wall angle were measured by means of proper optical measurements. These measurements were compared with theoretical values (135º and 1 mm respectively) and the difference between theoretical and experimental values represents the geometrical errors of the machined piece: angle error (y_1) and depth error (y_2). Both geometrical errors -y_1 and y_2- are considered as output parameters of each experiment.

5.2. The First Two Steps: Extracting the Relevant Internal Structures and Main Variables (Feature Selection)

5.2.1. Analysing the Internal Structure of a Data Set

As detailed in Section 2, PCA and CMLHL are two methods for identifying the internal structure of the data; both were applied to this industrial problem. Both methods have been applied to the three different case studies to know if the data sets are informative enough and also identified the most interesting underlying variables.

The following figures show the results of applying PCA (Figure 4.a, Figure 5.a and Figure 6.a) and CMLHL (Figure 4.b, Figure 5.b and Figure 6.b) in three different cases study. The vertical and horizontal axes forming these projections are combinations of the variables contained in the original data sets.

Figure 4. PCA projections (Figure 4.a) and CMLHL projections (Figure 4.b) for a steel piece.

By using Cooperative Maximum Likelihood Hebbian Learning (CMLHL) (Figure 4.b) it has been obtained a more sparse representation than with PCA (Figure 4.a). It can be easily seen how each group is formed by another 3 sub-groups and that the samples are clearly grouped and separated. CMLHL has identified three different groups or clusters (Figure 4.b) order by speed. After studying each cluster it is noted a second classification, which is based on the speed and frequency as it is shown in the right side of Figure 4.b.

Figure 5. PCA projections (Figure 5.a) and CMLHL projections (Figure 5.b) for an aluminium component.

CMLHL (Figure 5.b) has identified several clusters ordered by speed for aluminium components. It is worthy to note that, again, CMLHL is providing a more sparse visualization than PCA (Figure 5.a) and that this method has identified several clusters ordered by speed and frequency, and inside each cluster ordered by power.

Figure 6. PCA projections (Figure 6.a) and CMLHL projections (Figure 6.b) for a cooper piece.

As in the previous cases, it can be seen how CMLHL (Figure 6.b) has identified different cluster ordered by speed. For this material, five clusters have been identified and inside each clusters it is possible to notice another classification by frequency and power (Figure 6.b). Yet again, the use of PCA (Figure 6.a) is providing a five cluster projection but in less sparse and informative way than CMLHL (Figure 6.b).

As it can be seen in the previous figures (Figure 4, Figure 5 and Figure 6), both methods have identified a clear internal structure in the case of the three different materials as several well-defined clusters have been identified. It can be affirmed that CMLHL provides, in general, a sparser representation than PCA due to the combined use of MLHL based method and the application of lateral connections. As it is clear that there are several well-defined groups, the three data sets describing each material are informative enough, and it is possible to move to the second step of this model.

5.2.2. Feature Selection by CMLHL

By analysing the results obtained by CMLHL (Figure 4.b, Figure 5.b and Figure 6.b) of the three materials in the second step, it can be seen that, of the original data sets, the most significant variables to be processed in the third step are: power, speed and frequency. This leads to the application of the third phase or step of this process, which accurately and efficiently optimizes the model of the laser milling by applying several classical modelling systems.

Thus, for these three materials, the date sets describing each element are informative enough (first step). The main variables to be analysed (second step) in the third and final step of the presented model are the power, the speed and the frequency.

5.3. The Third Step: Applying System Identification for Modelling the Laser Milling Optimal Conditions

The different model learning methods used were implemented in Matlab© making use of its toolboxes—function libraries for Matlab: the System Identification Toolbox and the Control System Toolbox. The experiment followed the identification procedure detailed in Section 4.2.: the model structures were analysed to obtain the models that best suite the data set. The Akaike information criterion (AIC) was used to obtain the best degree of the model and its delay for each model structure. A total of 36 techniques were carried out to obtain the models, including:

- The frequency response analysis based on the spectrum analysis and the Fourier fast transform (FFT) were used to determine the data dynamics.
- The finite impulse response method (FIR) correlation analysis was used to determine the steady state conditions.
- The black-box models synthesis: up to 31 different combinations of model structure and optimization technique were considered, such as the least squares method, the QR factorization of ARX models and the recursive normalized gradient algorithm of RARMAX models (Ljung, 1999; Söderström and Stoica, 1989).

- Three different residual analysis based on cross correlation were carried out: the residual analysis between the residual $\hat{R}_{\varepsilon}^{N}(\tau)$, between the residual and the input $\hat{R}_{\varepsilon u}^{N}(\tau)$, and the non-linear residual correlation $\hat{R}_{\varepsilon^2 u^2}^{N}(\tau)$.

To validate the obtained models, several different indexes have been used. The indexes are recognized and widely-used measures in system identification (Ljung, 1999; Nörgaard et al., 2000; Söderström and Stoica, 1989).

- The percentage representation of the estimated model. This index is calculated as the normalized mean error for the one-step prediction (FIT1), for the ten-step prediction (FIT10) and with the ∞-step prediction (FIT). The FIT is known as simulation in classical system identification.
- The graphical representation of the FIT1 – $\hat{y}_1(t \mid m)$–, the FIT10 – $\hat{y}_{10}(t \mid m)$– and the FIT – $\hat{y}_{\infty}(t \mid m)$–.
- The loss function or error function (V): the numeric value of the mean squared error (MSE) that is computed with the estimation data set.
- The generalization error value: the numeric value of the normalized sum of squared errors (NSSE) that is computed with the validation data set.
- The final prediction error (FPE) is calculated as the average generalization error value computed with the estimation data set.

The results of modelling each of the three industrial processes are shown from Figure 7 to Figure 9 for cooper, aluminium and steel, respectively. The figures show the graphical representations for the best models found in each case. In all of them, the X-axis represents the number of samples used in the validation of the model, while the Y-axis represents the normalized output variable range, with the output variable being the angle error or the depth error of the test piece. In all the figures, the real operation condition is plotted as a solid line, and the estimated output of the model is plotted as a dotted line. The training and the validation data sets include 78 and 20 samples, respectively.

For milling cooper components, the best models found for both the angle error (see Table 1) and the depth error (see Table 2) are the ARX and the OE models, which are found to be totally equivalent according also to the results in Figure 7. These models not only present the lower loss function and generalization error values, but also the higher system representation indexes (FIT and FIT1). Finally, the polynomials parameters for the OE and the ARX models are presented in Table 3 and Table 4, respectively.

Figure 7. Milling of cooper components. The real measurement (solid line), the simulated output and the one-step prediction (dotted line) for OE and ARX models are shown.

Table 1. Milling of cooper components. Indicator values for several proposed models of the angle error.

Table 2. Milling of cooper components. Indicator values for several proposed models of the depth error.

Table 3. Milling of cooper components. Function and parameters that represent the behaviour of the laser-milled piece for the angle error. The degree of the OE model polynomials are $n_{b1}=1$, $n_{b2}=4$, $n_{b3}=1$, $n_f=1$, $n_{k1}=1$, $n_{k2}=3$, $n_{k3}=1$. [1 4 1 1 1 3 1].

Table 4. Milling of cooper components. Function and parameters that represent the behaviour of the laser-milled piece for the depth. The degree of the ARX model polynomials are $n_a=1$, $n_{b1}=1$, $n_{b2}=4$, $n_{b3}=1$, $n_{k1}=1$, $n_{k2}=3$, $n_{k3}=1$. [1 1 4 1 1 3 1].

The same reasoning is followed for the aluminium and the hardened steel components. The best models found indexes values are presented in Table 5 and Table 6 for the aluminium components and in Table 9 and Table 10 for hardened steel, for the angle and depth errors respectively. In the case of aluminium components, the best models found are the OE and BJ models shown in Table 7 and Table 8.

From the graph (Figure 8), it can be concluded that the BJ model is the best model for simulating and predicting the behaviour of the laser milled with an aluminium test piece for both outputs: the angle error and the depth error, as they meet the indicators and are capable of modelling more than 99% of the true measurements.

Figure 8. Milling of aluminium components. Representation of the real measurement (solid line), the simulated output and the one-step prediction (dotted line) for OE and BJ models.

Table 5. Milling of aluminium components. Indicator values for several proposed models of the angle error

Table 6. Milling of aluminium components. Indicator values for several proposed models of the depth error.

Table 7. Milling of aluminium components. Function and parameters that represent the behaviour of the laser-milled piece for the angle error. The degree of the BJ model polynomials are $n_{b1}=3$, $n_{b2}=1$, $n_{b3}=1$, $n_c=3$, $n_d=2$,$n_f=2$, $n_{k1}=2$, $n_{k2}=1$, $n_{k3}=1$. [3 1 1 3 2 2 2 1 1].

Table 8. Milling of aluminium components. Function and parameters that represent the behaviour of the laser-milled piece for the depth error. The degree of the BJ model polynomials are $n_{b1}=1$, $n_{b2}=3$, $n_{b3}=1$, $n_c=3$, $n_d=2$, $n_f=2$, $n_{k1}=1$, $n_{k2}=3$, $n_{k3}=1$. [1 3 1 3 2 2 1 3 1].

For hardened steel components, the best models are presented in Table 9 and Table 10 for the angle error and the depth error, respectively; while Figure 9 shows the one-step prediction and the simulated output for the OE and the BJ models.

From the graph (Figure 9.a, Figure 9.b), it can be concluded that the BJ model is the best model for simulating and predicting the behaviour of the laser-milled test piece of steal for angle error better than the OE model. Also, the BJ and OE models (Figure 9.c, Figure 9.d) are capable of simulating and predicting the behaviour of the laser-milled piece of steal for depth error in the same manner (See also Table 10). All these models are capable of modelling more than 99% of the true measurements. The comparison of the best models found is shown in Table 9 and Table 10 by model function and type. The chosen BJ and OE models are detailed in Table 11 and Table 12.

Figure 9. Milling hardened steel components. Representation of the real measurement (solid line), the simulated output and the one-step prediction (dashed line) for OE and BJ models.

Table 9. Milling hardened steel components. Indicator values for several proposed models of the angle error.

Table 10. Milling hardened steel components. Indicator values for several proposed models of the depth error.

Table 11. Milling hardened steel components. Function and parameters that represent the behaviour of the laser-milled piece for the angle error. The degree of the BJ model polynomials are $n_{b1}=1$, $n_{b2}=1$, $n_{b3}=1$, $n_c=2$, $n_d=2$, $n_f=2$, $n_{k1}=1$, $n_{k2}=1$, $n_{k3}=1$. [1 1 1 2 2 2 1 1 1].

Table 12. Milling hardened steel components. Function and parameters that represent the behaviour of the laser-milled piece for the depth error of the test piece. The degree of the OE model polynomials are $n_{b1}=1$, $n_{b2}=2$, $n_{b3}=1$, $n_f=2$, $n_{k1}=1$, $n_{k2}=2$, $n_{k3}=1$. [1 2 1 2 1 2 1].

The obtained models can be used not only to predict the angle error and the depth error of the test piece, but also to determine the optimal conditions to minimize the error: considering that it is a polynomial model, if all but one input variable are fixed, the remaining variables could be calculated and fixed to minimize the angle error and the depth error of the test piece on the flat metallic piece of cooper, aluminium and steel. So, in Figure 10, a graph of the errors in the flat metallic piece of aluminium is shown related to the others three input components: power, speed and frequency.

Figure 10 shows the output response of the two different errors: the angle error (Figure 10.a) and depth error (Figure 10.b) for different input variable ranges. The angle error and the depth can be zero for different values of power and speed for a constant value of frequency; i.e., it is possible to achieve an angle error of zero for a laser power of 90% and a milling speed of 460 mm/s. The X-axis shows the variable range of power $u_1(t)$, from 50 to 100, as a percentage of the maximum power performed by the laser (%) and the Y-axis represents the variable range of speed $u_2(t)$, from 225 to 525, in mm/s. The variable frequency $u_3(t)$ is fixed at 85 kHz. The errors of the test piece are shown on the bars, which are distributed from -0.4 to 0.1 degrees and from -0.05 to 0.25 mm for the angle error $y_1(t)$ and the depth error $y_2(t)$, respectively.

Figure 10. Output response of two different errors: the angle error (Figure 10.a) and the depth error (Figure 10.b) for different input variable ranges.

6. Conclusions and Future Work

This interdisciplinary research has presented a detailed study for designing a three-step soft computing procedure to identify the most appropriate modelling system to solve a real-life industrial problem: the laser milling of metal components. The procedure has been validated with three different materials: aluminium, cooper and hardened steel. It is worth mentioning that with classical and soft computing techniques, two interesting variables such as the angle error and the depth error have been successfully modelled.

The purpose of this solution is to assist end-users in choosing the correct operating conditions of the tools, in this case, a laser mill. The main advantage of this proposal is that by using the obtained model, operators only need to provide values for a small number of input variables out of the whole input set to obtain the angle and the depth values of the tool or piece, which are the final operating parameters and the most difficult ones to estimate. Thus, an important decrease in operation start-up costs is obtained.

Future work will focus on the study and application of this model to other kinds of materials of industrial interest, such as cast single-crystal nickel super-alloys for high-pressure turbine blades, and also on the application of this model to the optimization of different but similar industrial problems, such as laser cladding, laser super-polishing and laser drilling. Another interesting application and real-world, large-scale scenario is in medical therapeutics (odonto-stomatology) for bucco-dental rehabilitation and restoration in the processing and manufacturing of bucco-dental prosthesis, such as partial crowns, inlays and onlays, and partial and complete prosthesis fitted on structures of different metals, such as titanium, chrome cobalt, noble metals, etc., in which the optimising of the registering and mapping of the surgical field to be operated on is required.

In addition, the analysis of different connectionist models will be applied for feature selection.

Acknowledgments

This research has been partially supported through the *Junta de Castilla y León's* project BU006A08 and the Spanish Ministry of Science and Technology's project [TIN2008-06681-C06-04]. The authors would also like to thank the manufacturer of components for vehicle interiors, Grupo Antolin Ingeniería, S.A. as part of the MAGNO 2008 - 1028.- CENIT Project funded by the Spanish Ministry of Science and Innovation.

References

Akaike, H. (1969). Fitting autoregressive models for prediction, *Annals of the Institute of Statistical Mathematics*, 20, 425–439.

Avci, E. (2007). A new optimum feature extraction and classification method for speaker recognition: Gwpnn. *Expert Systems with Applications*, 32 (2), 485 – 498.

Avci, E., Sengur, A., and Hanbay, D. (2009). An optimum feature extraction method for texture classification. *Expert Systems with Applications*, 36 (3, Part 2), 6036 – 6043.

Bertsekas, D. (1999). *Nonlinear Programming*. Athena Scientific, Belmont, MA.

Caló, D. G. (2007). Gaussian mixture model classification: A projection pursuit approach. *Computational Statistics & Data Analysis*, 52 (1), 471 – 482.

Chen, C., Lee, H., and Chang, Y. (2009). Two novel feature selection approaches for web page classification. *Expert Systems with Applications*, 36 (1), 260 – 272.

Corchado, E., D.MacDonald, and Fyfe, C. (2004). Maximum and minimum likelihood hebbian learning for exploratory projection pursuit. *Data Mining and Knowledge Discovery*, 8 (3), 203–225.

Corchado, E. and Fyfe, C. (2003). Connectionist techniques for the identification and suppression of interfering underlying factors. *International Journal of Pattern Recognition and Artificial Intelligence*, 17 (8), 1447–1466.

Corchado, E., Han, Y., and Fyfe, C. (2003). Structuring global responses of local filters using lateral connections. *Journal of Experimental & Theoretical Artificial Intelligence*, 15 (4), 473–487.

da Silva, A., Neto, J., Nagem, N., and Freixo, N. (2009). Parametric ARX modeling of the electrolytic smelter pot. In *UKSIM '09: Proceedings of the UKSim 2009: 11th International Conference on Computer Modelling and Simulation*, Washington, DC, USA: IEEE Computer Society, pp. 217–222.

Datong, L., Yu, P., and Xiyuan, P. (2009). Online fault prediction based on combined AOSVR and ARMA models. In *Testing and Diagnosis, 2009. ICTD 2009*, New York, USA: *IEEE Circuits and Systems International Conference,* pp. 1–4.

Diaconis, P. and Freedman, D. (1984). Asymptotics of graphical projections. *The Annals of Statistics*, 12(3), 793–815.

Esbensen, K. and Geladi, P. (2009). Principal component analysis: Concept, geometrical interpretation, mathematical background, algorithms, history, practice. In Brown, S. D., Tauler, R., and Walczak, B., editors, *Comprehensive Chemometrics*, Oxford: Elsevier, pp. 211 – 226.

Fernandes, C., Comon, P., and Favier, G. (2010). Blind identification of MISO-FIR channels. *Signal Processing*, 90 (2), 490 – 503.

Földiák, P. (1992). *Models of Sensory Coding*. PhD thesis, University of Cambridge.

Friedman, J. and Tukey, J. (1974). Projection pursuit algorithm for exploratory data-analysis. *IEEE Transactions on Computers*, 23 (9), 881–890.

Fyfe, C. (1993). PCA properties of interneurons: from neurobiology to real world computing. In *International Conference on Artificial Neural Networks:* Springer Verlag, pp. 183–188.

Gavrilis, D., Tsoulos, I. G., and Dermatas, E. (2008). Selecting and constructing features using grammatical evolution. *Pattern Recognition Letters*, 29 (9), 1358 – 1365.

Gillberg, J. and Ljung, L. (2010). Frequency domain identification of continuous-time output error models, part II: Non-uniformly sampled data and B-spline output approximation. *Automatica*, 46 (1), 11–18.

Gonzalez, F., Munoz, L., and Belanche, A. (2009). Gene subset selection in microarray data using entropic filtering for cancer classification. *Expert Systems*, 26 (1), 113–124.

Guyon, I. and Elisseeff, A. (2003). An introduction to variable and feature selection. *Journal of Machine Learning Research, Special Issue on Variable and Feature Selection*, 3, 1157–1182.

Haber, R. and Keviczky, L. (1999a). *Nonlinear System Identification. Input-Output Modeling Approach. Part 1: Nonlinear System Parameter Estimation*. Kluwer Academic Publishers.

Haber, R. and Keviczky, L. (1999b). *Nonlinear System Identification. Input-Output Modeling Approach. Part 2: Nonlinear System structure Identification*. Kluwer Academic Publishers.

Harrison, P. M., Paul, M., Henry, M., Henderson, I., and Brownell, M. (2004). Laser milling of metallic and nonmetallic substrates in the nanosecond regime with Q-switched diode pumped solid state lasers. In *High-Power Laser Ablation V*. Proceedings of the Society of Photo-optical Instrumentation Engineers: SPIE, Vol. 5448, pp. 624–633.

Henry, M., Harrison, P., Henderson, I., and Brownell, M. (2004). Laser milling - a practical industrial solution for machining a wide variety of materials. In *5th International Symposium on Laser Precision Microfabrication*. Proceedings of the Society of Photo-optical Instrumentation Engineers, Nara, Japan: SPIE, Vol. 5662, pp. 627–632.

Herrero, A., Corchado, E., Sáiz, L., and Abraham, A. (2010). DIPKIP: A connectionist knowledge management system to identify knowledge deficits in practical cases. *Computational Intelligence*, 26 (1), 26–56.

Hotelling, H. (1933). Analysis of a complex of statistical variables into principal components. *Journal of Education Psychology*, 24, 417–444.

Huang, J., Luo, H., Long, B., and Wang, H. (2009). Prediction research about small sample failure data based on ARMA model. In *Testing and Diagnosis, 2009. ICTD 2009. IEEE Circuits and Systems International Conference on*, New York, USA, pp. 1–6.

Ion, J. (2005). Laser processing of engineering materials: Principles, procedure and industrial application. *Butterworth-Heinemann*, pp. 456–475.

Iqbal, M., Sundararaj, U., and Shah, S. (2010). New approach to develop dynamic gray box model for a plasticating twin-screw extruder. *Industrial & Engineering Chemistry Research*, 49 (2), 648–657.

Ismail, N., Tajjudin, N., Rahiman, M., and Taib, M. (2009). Modeling of dynamic response of essential oil extraction process. In *Signal Processing Its Applications, 2009. 5th International Colloquium on*, New York, USA: CSPA, pp. 298 –301.

Kim, K.J. and Cho, S.B. (2006). Ensemble classifiers based on correlation analysis for DNA microarray classification. *Neurocomputing*. Neural Networks - Selected Papers from the 7th Brazilian Symposium on Neural Networks (SBRN '04), 7th Brazilian Symposium on Neural Networks, 70 (1-3), 187-199

Kuhl, M. (2002). From macro to micro -the development of laser ablation. In *International Congress on Applications of Lasers & Electro Optics (ICALEO)*, Scottsdale, Arizona USA.

Liu, H., Sun, J., Liu, L., and Zhang, H. (2009a). Feature selection with dynamic mutual information. *Pattern Recognition*, 42 (7), 1330-1339.

Liu, H. and Yu, L. (2005). Toward integrating feature selection algorithms for classification and clustering. *IEEE Educational Activities Department,* 17(4), 491-502.

Liu, Y., Liu, Y., and Chan, K. C. (2009b). Dimensionality reduction for heterogeneous dataset in rushes editing. *Pattern Recognition*, 42 (2), 229-242. Learning Semantics from Multimedia Content.

Ljung, L. (1999). *System Identification. Theory for the User*. Prentice-Hall, Upper Saddle River, N.J., USA, 2nd edition.

Malpica, J. A., Rejas, J. G., and Alonso, M. C. (2008). A projection pursuit algorithm for anomaly detection in hyperspectral imagery. *Pattern Recognition*, 41 (11), 3313-3327.

Marinakis, Y., Marinaki, M., Dounias, G., Jantzen, J., and Bjerregaard, B. (2009). Intelligent and nature inspired optimization methods in medicine: the Pap smear cell classification problem. *Expert Systems*, 26 (5), 433-457.

Meiler, A., Schimida, O., Schudy, M., and Hofer, E. (2008). Dynamic fuel cell stack model for real-time simulation based on system identification. *Journal of Power Sources*, 176 (2), 523-528.

Mustafaraj, G., Chen, J., and Lowry, G. (2010). Development of room temperature and relative humidity linear parametric models for an open office using BMS data. *Energy and Buildings*, 42 (3), 348-356.

Mostafa, M. and Billor, N. (2009). Recognition of western style musical genres using machine learning techniques. *Expert Systems with Applications*, 36 (8), 11378-11389.

Nelles, O. (2001). *Nonlinear System Identification. From Classical Approaches to Neural Networks and Fuzzy Models*. Springer, Berlin, Germany.

Nörgaard, M., Ravn, O., Poulsen, N., and Hansen, L. (2000). *Neural Networks for Modelling and Control of Dynamic Systems*. Springer-Verlag, London U.K.

Oja, E. (1982). A simplified neuron model as a principal component analyzer. *Journal of Mathematical Biology*, 15 (3), 267-273.

Pearson, K. (1901). On lines and planes of closest fit to systems of points in space. *Philosophical Magazine*, 2 (6), 559-572.

Raducanu, B., VitriÃ , J., and Leonardis, A. (2010). Online pattern recognition and machine learning techniques for computer-vision: Theory and applications. *Image and Vision Computing*, In Press.

Seung, H., Socci, N., and Lee, D. (1998). The Rectified Gaussian Distribution. *Advances in Neural Information Processing Systems*, 10, 350-356.

Söderström, T. and Stoica, P. (1989). *System identification*. Prentice Hall International, Englewood Cliffs, NJ.

Su, T.H., Zhang, T.W., Guan, D.J., and Huang, H.J. (2009). Off-line recognition of realistic chinese handwriting using segmentation-free strategy. *Pattern Recognition*, 42 (1), 167-182.

Taghavi, N. and Sadr, A. (2008). Piezoelectric transducer modeling: with system identification (SI) method. In *Proceedings of World Academy of Science, Engineering and Technology*, Bangkok, Thailand, Vol. 29, pp. 296-301.

Tani, G., Orazi, L., Fortunato, A., and Cuccolini, G. (2008). Laser ablation of metals: A 3D process simulation for industrial applications. Journal of Manufacturing Science and Engineering, 130 (3), 31111–31122.

Valeriana-Garcia, R., Fernandez-Breis, J., Ruiz-Martinez, J., Garcia-Sanchez, F., and Martinez-Bejar, R. (2008). A knowledge acquisition methodology to ontology construction for information retrieval from medical documents. *Expert Systems*, 25 (3), 314-334.

Wang, R. and Cheng, W. (2009). Using armax-egarch model to forescast day-ahead electricity prices for pjm market, flushing. *Scientific & Technical Development Inc*.

Witte, R., Moser, T., Liebers, R., and Holtz, R. (2008). Laser micro-drilling with nanoseconds: parametrical influences and results. In Manuf, J., editor, *Advanced Laser Technologies*. Proceedings of the Photo-Optical Instrumentation Engineering , Conference on Advanced Laser Technologies, Levi, Finland: SPIE, Vol. 7022, pp. 702208-702216.

Wolczowski, A. and Kurzynski, M. (2010). Human-machine interface in bioprosthesis control using EMG signal classification. *Expert Systems*, 27 (1), 53-70.

Wright, J., Yang, A., and Ganesh, A. (2009). Robust Face Recognition via Sparse Representation. *IEEE Transactions on Pattern Analisys and Machine Intelligence*, 31 (2), 210-227.

FIGURE INDEX

Figure 1. The A matrix for the Rectified Gaussian network with 24 outputs. Black squares are negative, white are positive and the shading in each square is proportional to the weight size.

Figure 2. Lateral connections between neighbouring outputs.

Figure 3. The flow chart of the proposed procedure.

Figure 4. PCA projections (Figure 4.a) and CMLHL projections (Figure 4.b) for a steel piece.

Figure 5. PCA projections (Figure 5.a) and CMLHL projections (Figure 5.b) for an aluminium component.

Figure 6. PCA projections (Figure 6.a) and CMLHL projections (Figure 6.b) for a cooper piece.

Figure 7. Milling of cooper components. The real measurement (solid line), the simulated output and the model prediction (dotted line) for the OE and ARX models are shown.

Figure 8. Milling of aluminium components. Representation of the real measurement (solid line), the simulated output and the model prediction (dotted line) for OE and BJ models.

Figure 9. Milling hardened steel components. Representation of the real measurement (solid line), the simulated output and the model prediction (dotted line) for OE and BJ models.

Figure 10. Output response of two different errors: the angle error (Figure 10.a) and the depth error (Figure 10.b) for different input variable ranges.

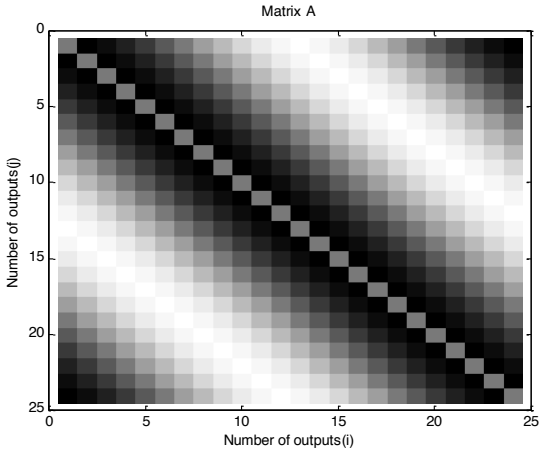

Figure 1. The A matrix for the Rectified Gaussian network with 24 outputs. Black squares are negative, white are positive and the shading in each square is proportional to the weight size.

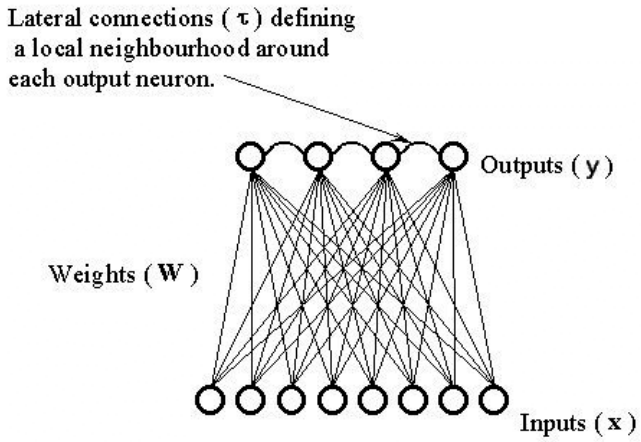

Figure 2. Lateral connections between neighbouring outputs.

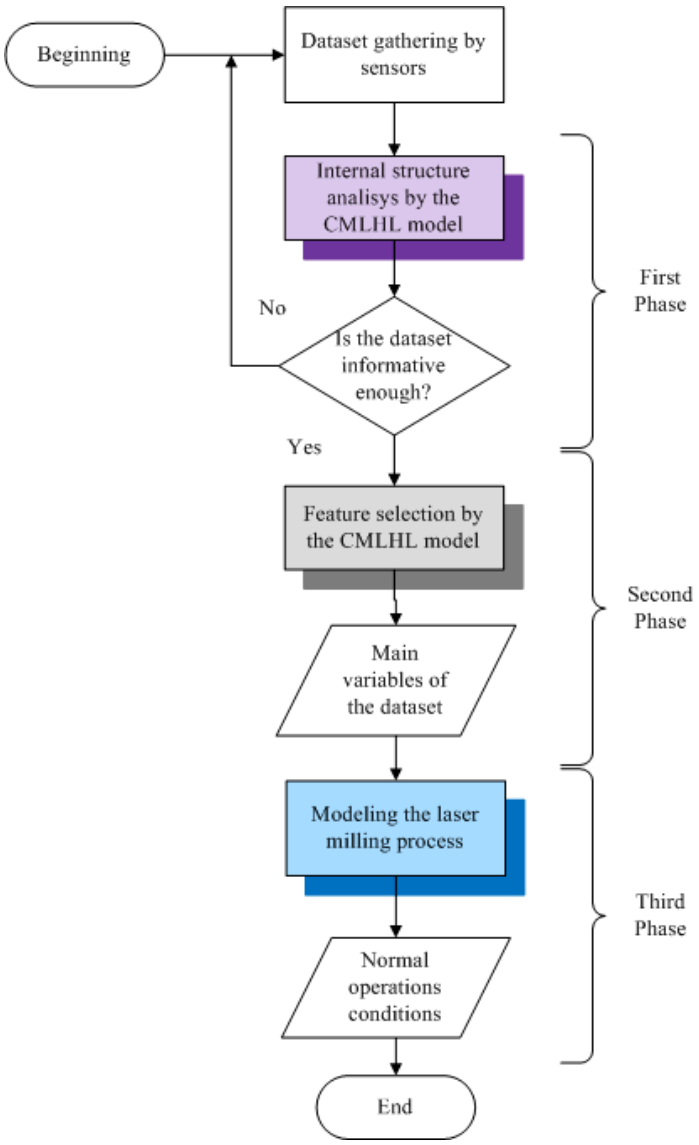

Figure 3. The flow chart of the proposed procedure.

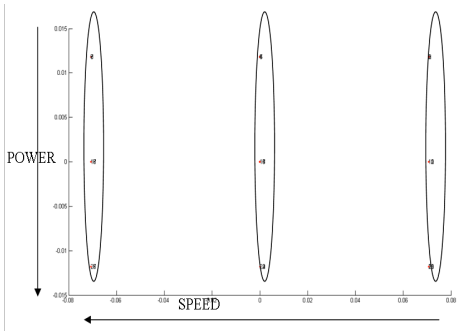

Figure 4.a. PCA projections.

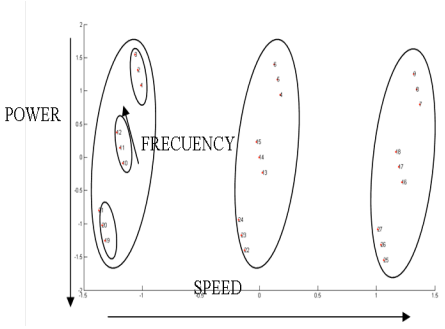

Figure 4.b. CMLHL projections.

Figure 4. PCA projections (Figure 4.a) and CMLHL projections (Figure 4.b) for a steel piece.

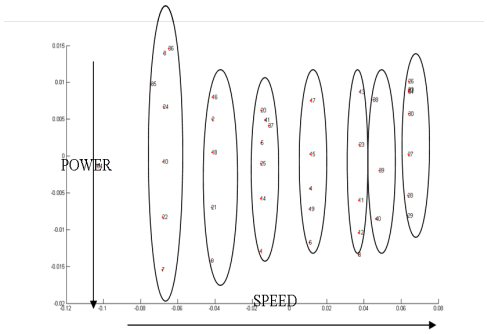

Figure 5.a. PCA projections.

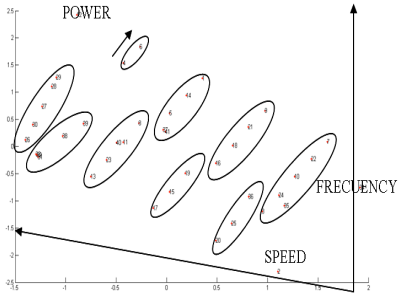

Figure 5.b. CMLHL projections.

Figure 5. PCA projections (Figure 5.a) and CMLHL projections (Figure 5.b) for an aluminium component.

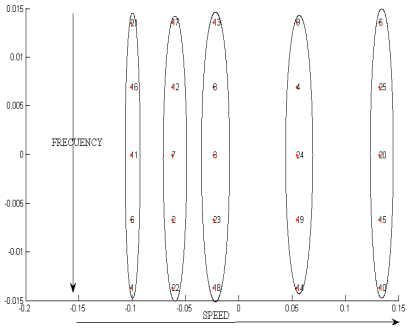

Figure 6.a. PCA projections.

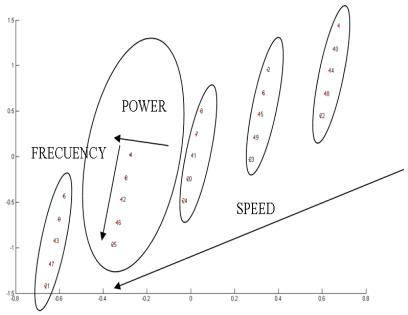

Figure 6.b. CMLHL projections.

Figure 6. PCA projections (Figure 6.a) and CMLHL projections (Figure 6.b) for a cooper piece.

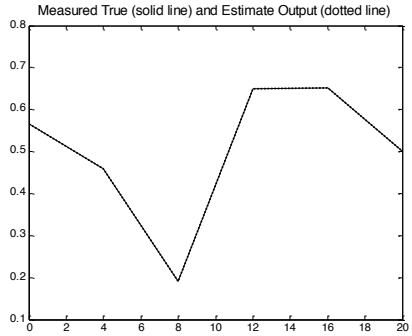

Figure 7.a. OE and ARX models for the angle error.

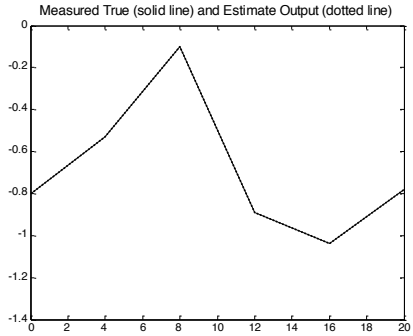

Figure 7.b. OE and ARX models for the depth error.

Figure 7. Milling of cooper components. The real measurement (solid line), the simulated output and the one-step prediction (dotted line) for the OE and ARX models are shown.

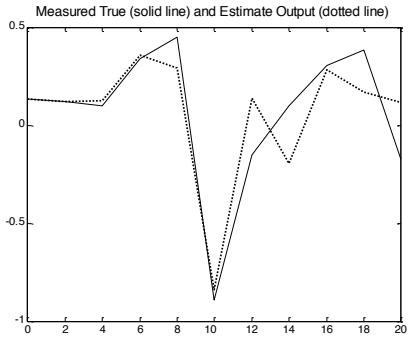

Figure 8.a. OE model for the angle error.

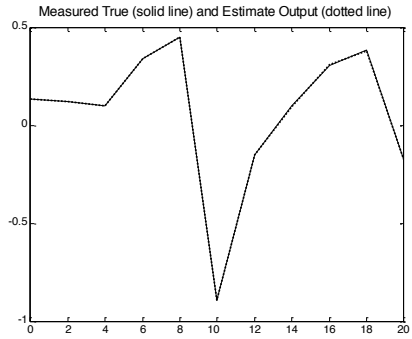

Figure 8.b. BJ model for the angle error.

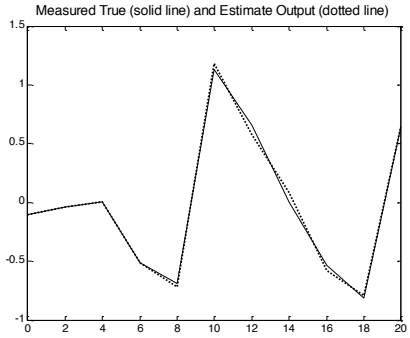

Figure 8.c. OE model for the depth error.

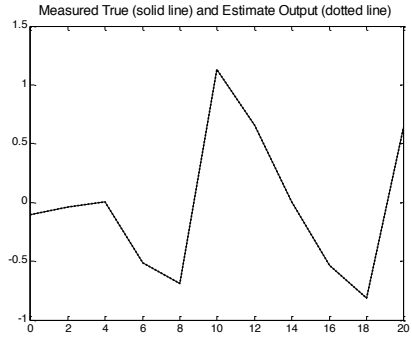

Figure 8.d. BJ model for the depth error.

Figure 8. Milling of aluminium components. Representation of the real measurement (solid line), the simulated output and the model prediction (dotted line) for the OE and BJ models.

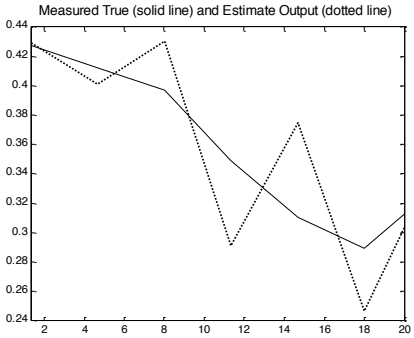

Figure 9.a. OE model for the angle error.

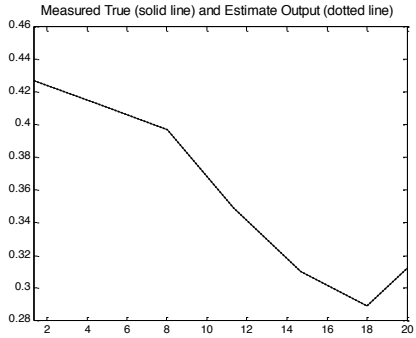

Figure 9.b. BJ model for the angle error.

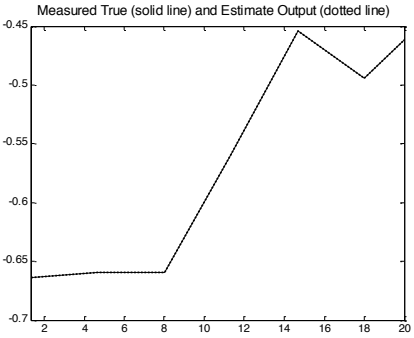

Figure 9.c. OE model for the depth error.

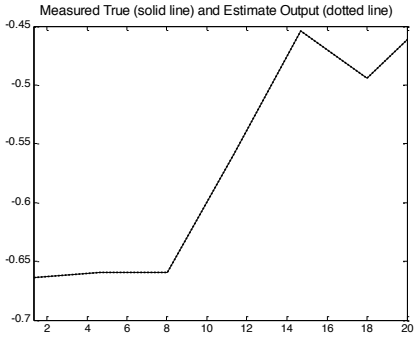

Figure 9.d. BJ model for the depth error.

Figure 9. Milling hardened steel components. Representation of the real measurement (solid line), the simulated output and the model prediction (dotted line) for the OE and BJ models.

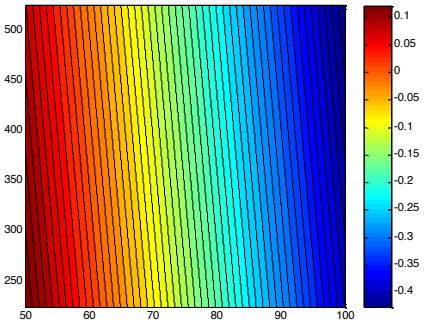

Figure 10.a. Output response for the angle error.

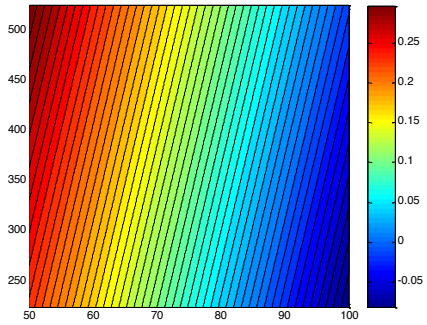

Figure 10.b. Output response for the depth error.

Figure 10. Output response of two different errors: the angle error (Figure 10.a) and the depth error (Figure 10.b) for different input variable ranges.

Expert Systems: The Journal of Knowledge Engineering, Special Issue on Statistical, Soft and Structural Methods of Pattern Recognition (CORES 2009)

TABLE INDEX

Table 1. Milling if cooper components. Indicator values for several proposed models of the angle error.

Table 2. Milling of cooper components. Indicator values for several proposed models of the depth error.

Table 3. Milling of cooper components. Function and parameters that represent the behaviour of the laser-milled piece for the angle error. The degree of the OE model polynomials are $n_{b1}=1$, $n_{b2}=4$, $n_{b3}=1$,$n_f=1$, $n_{k1}=1$, $n_{k2}=3$, $n_{k3}=1$. [1 4 1 1 1 3 1].

Table 4. Milling of cooper components. Function and parameters that represent the behaviour of the laser-milled piece for the depth. The degree of the ARX model polynomials are $n_a=1$, $n_{b1}=1$, $n_{b2}=4$, $n_{b3}=1$, $n_{k1}=1$, $n_{k2}=3$, $n_{k3}=1$. [1 1 4 1 1 3 1].

Table 5. Milling aluminium components. Indicator values for several proposed models of the angle error.

Table 6. Milling aluminium components. Indicator values for several proposed models of the depth error.

Table 7. Milling aluminium components. Function and parameters that represent the behaviour of the laser-milled piece for the angle error. The degree of the BJ model polynomials are $n_{b1}=3$, $n_{b2}=1$, $n_{b3}=1$, $n_c=3$, $n_d=2$, $n_f=2$, $n_{k1}=2$, $n_{k2}=1$, $n_{k3}=1$. [3 1 1 3 2 2 2 1 1].

Table 8. Milling aluminium components. Function and parameters that represent the behaviour of the laser-milled piece for the depth error. The degree of the BJ model polynomials are $n_{b1}=1$, $n_{b2}=3$, $n_{b3}=1$, $n_c=3$, $n_d=2$, $n_f=2$, $n_{k1}=1$, $n_{k2}=3$, $n_{k3}=1$. [1 3 1 3 2 2 1 3 1].

Table 9. Milling hardened steel components. Indicator values for several proposed models of the angle error.

Table 10. Milling hardened steel components. Indicator values for several proposed models of the depth error.

Table 11. Milling hardened steel components. Function and parameters that represent the behaviour of the laser-milled piece for the angle error. The degree of the BJ model polynomials are $n_{b1}=1$, $n_{b2}=1$, $n_{b3}=1$, $n_c=2$, $n_d=2$, $n_f=2$, $n_{k1}=1$, $n_{k2}=1$, $n_{k3}=1$. [1 1 1 2 2 2 1 1 1].

Table 12. Milling hardened steel components. Function and parameters that represent the behaviour of the laser-milled piece for the depth error of the test piece. The degree of the OE model polynomials are $n_{b1}=1$, $n_{b2}=2$, $n_{b3}=1$, $n_f=2$, $n_{k1}=1$, $n_{k2}=2$, $n_{k3}=1$. [1 2 1 2 1 2 1].

Table 1. Milling of cooper components. Indicator values for several proposed models of the angle error.

Model	Performance Indexes
Black-box OE model with $n_{b1}=1$, $n_{b2}=4$, $n_{b3}=1$, $n_f=1$, $n_{k1}=1$, $n_{k2}=2$, $n_{k3}=1$. The model is estimated using the prediction error method; the degree of the model selection is carried out from the best AIC criterion (the structure that minimizes AIC).	FIT: 100%, FIT1: 100% FIT10: 100%, V: 0.066 FPE: 1.1302, NSSE: 7.46e-31 Variance of e(t): 0.598
Black-box OE model with $n_{b1}=1$, $n_{b2}=4$, $n_{b3}=1$, $n_f=1$, $n_{k1}=1$, $n_{k2}=3$, $n_{k3}=1$. The model is estimated using the prediction error method; the degree of the model selection is carried out with the best AIC criterion (the structure that minimizes AIC).	FIT: 100%, FIT1: 100% FIT10: 100%, V: 0.011 FPE: 0.413, NSSE: 3.76e-30 Variance of e(t): 0.212
Black-box ARX model with $n_a=1$, $n_{b1}=1$, $n_{b2}=4$, $n_{b3}=1$, $n_{k1}=1$, $n_{k2}=2$, $n_{k3}=1$. The model is estimated using the least squares method, QR factorization; the degree of the model selection is carried out with the best AIC criterion (the structure that minimizes AIC).	FIT: 18.34%, FIT1: 11.13% FIT10: 11.13%, V: 0.066 FPE: 0.1514, NSSE: 0.019
Black-box ARX model with $n_a=1$, $n_{b1}=1$, $n_{b2}=4$, $n_{b3}=1$, $n_{k1}=1$, $n_{k2}=3$, $n_{k3}=1$. The model is estimated using the least squares method, QR factorization; the degree of the model selection is carried out with the best AIC criterion (the structure that minimizes AIC).	FIT: 100%, FIT1: 100% FIT10: 100%, V: 0.061 FPE: 0.139, NSSE: 1.68e-28 Variance of e(t): 0.22

Table 2. Milling of cooper components. Indicator values for several proposed models of the depth error.

Model	Performance Indexes
Black-box OE model with $n_{b1}=1$, $n_{b2}=4$, $n_{b3}=1$, $n_f=1$, $n_{k1}=1$, $n_{k2}=2$, $n_{k3}=1$. The model is estimated using the prediction error method; the degree of the model selection is carried out from the best AIC criterion (the structure that minimizes AIC).	FIT: 100%, FIT1: 100% FIT10: 100%, V: 0.083 FPE: 1.42, NSSE: 1.21e-29 Variance of e(t): 0.755
Black-box OE model with $n_{b1}=1$, $n_{b2}=4$, $n_{b3}=1$, $n_f=1$, $n_{k1}=1$, $n_{k2}=3$, $n_{k3}=1$. The model is estimated using the prediction error method; the degree of the model selection is carried out with the best AIC criterion (the structure that minimizes AIC).	FIT: 100%, FIT1: 100% FIT10: 100%, V: 0.029 FPE: 1.047, NSSE: 2.63e-29 Variance of e(t): 0.538
Black-box ARX model with $n_a=1$, $n_{b1}=1$, $n_{b2}=4$, $n_{b3}=1$, $n_{k1}=1$, $n_{k2}=2$, $n_{k3}=1$. The model is estimated using the least squares method, QR factorization; the degree of the model selection is carried out with the best AIC criterion (the structure that minimizes AIC).	FIT: 43.58%, FIT1: 42.33% FIT10: 42.33%, V: 0.101 FPE: 0.2315, NSSE: 0.0308
Black-box ARX model with $n_a=1$, $n_{b1}=1$, $n_{b2}=4$, $n_{b3}=1$, $n_{k1}=1$, $n_{k2}=3$, $n_{k3}=1$. The model is estimated using the least squares method, QR factorization; the degree of the model selection is carried out with the best AIC criterion (the structure that minimizes AIC).	FIT: 100%, FIT1: 100% FIT10: 100%, V: 0.087 FPE: 0.198, NSSE: 3.60e-30 Variance of e(t): 0.313

Table 3. Milling of cooper components. Function and parameters that represent the behaviour of the laser-milled piece for the angle error. The degree of the OE model polynomials are $n_{b1}=1$, $n_{b2}=4$, $n_{b3}=1$,$n_f=1$, $n_{k1}=1$, $n_{k2}=3$, $n_{k3}=1$. [1 4 1 1 1 3 1].

Parameters and polynomials.	
$B1(q) = 0.03695\ q^{-1}$	$F1(q) = 1 + 0.6718\ q^{-1}$
$B2(q) = -0.0001911\ q^{-3} + 0.000186\ q^{-4} - 0.0002806\ q^{-5} + 0.001646\ q^{-6}$	$F2(q) = 1 + 0.5765\ q^{-1}$
$B3(q) = -0.01592\ q^{-1}$	$F3(q) = 1 + 0.9986\ q^{-1}$ *e(t) is white noise signal with variance 0.21*

Table 4. Milling of cooper components. Function and parameters that represent the behaviour of the laser-milled piece for the depth. The degree of the ARX model polynomials are $n_a=1, n_{b1}=1$, $n_{b2}=4$, $n_{b3}=1, n_{k1}=1$, $n_{k2}=3$, $n_{k3}=1$. [1 1 4 1 1 3 1].

Parameters and polynomials.	
$A1(q) = 1 + 0.5261\ q^{-1}$	$B1(q) = -0.04465\ q^{-1}$
$B2(q) = 0.0006061\ q^{-3} + 0.0002783\ q^{-4} + 0.0001222\ q^{-5} - 0.001414\ q^{-6}$	$B3(q) = 0.01051\ q^{-1}$ *e(t) is white noise signal with variance 0.31*

Table 5. Milling of aluminium components. Indicator values for several proposed models of the angle error.

Model	Performance Indexes
Black-box OE model with $n_{b1}=2$, $n_{b2}=2$, $n_{b3}=1$, $n_f=2$, $n_{k1}=2$, $n_{k2}=2$, $n_{k3}=1$. The model is estimated using the prediction error method; the degree of the model selection is carried out from the best AIC criterion (the structure that minimizes AIC).	FIT: 30.73%, FIT1: 30.73% FIT10: 30.73%, V: 0.117 FPE: 0.471, NSSE: 0.0617
Black-box OE model $n_{b1}=3$, $n_{b2}=1$, $n_{b3}=1$, $n_f=2$, $n_{k1}=2$, $n_{k2}=1$, $n_{k3}=1$. The model is estimated using the prediction error method; the degree of the model selection is carried out with the best AIC criterion (the structure that minimizes AIC).	FIT: 51.76%, FIT1: 51.76% FIT10: 51.76%, V: 0.1932 FPE: 0.80, NSSE: 0.0299
Black-box BJ model with $n_{b1}=2$, $n_{b2}=2$, $n_{b3}=1$, $n_c=3$, $n_d=2$, $n_f=2$, $n_{k1}=2$, $n_{k2}=2$, $n_{k3}=1$. The model is estimated using the prediction error method; the degree of the model selection is carried out with the best AIC criterion (the structure that minimizes AIC).	FIT: 44.44%, FIT1: 64.41% FIT10: 36.81%, V: 0.053 FPE: 0.588, NSSE: 0.016
Black-box BJ model with $n_{b1}=3$, $n_{b2}=1$, $n_{b3}=1$, $n_c=3$, $n_d=2$, $n_f=2$, $n_{k1}=2$, $n_{k2}=1$, $n_{k3}=1$. The model is estimated using the prediction error method; the degree of the model selection is carried out with the best AIC criterion (the structure that minimizes AIC).	FIT: 99.53%, FIT1: 99.41% FIT10: 99.53%, V: 0.104 FPE: 1,46, NSSE: 4.49e-6

Table 6. Milling of aluminium components. Indicator values for several proposed models of the depth error.

Model	Performance Indexes
Black-box OE model with $n_{b1}=2$, $n_{b2}=2$, $n_{b3}=1$, $n_f=2$, $n_{k1}=2$, $n_{k2}=2$, $n_{k3}=1$. The model is estimated using the prediction error method; the degree of the model selection is carried out from the best AIC criterion (the structure that minimizes AIC).	FIT: 61.09%, FIT1: 61.09% FIT10: 61.09%, V: 0.296 FPE: 1.18, NSSE: 0.0526
Black-box OE model with$n_{b1}=1$, $n_{b2}=3$, $n_{b3}=1$, $n_f=2$, $n_{k1}=1$, $n_{k2}=3$, $n_{k3}=1$. The model is estimated using the prediction error method; the degree of the model selection is carried out with the best AIC criterion (the structure that minimizes AIC).	FIT: 92.98%, FIT1: 92.98% FIT10: 92.98%, V: 0.174 FPE: 0.874, NSSE: 0.0017
Black-box BJ model with $n_{b1}=2$, $n_{b2}=2$, $n_{b3}=1$, $n_c=3$, $n_d=2$, $n_f=2$, $n_{k1}=2$, $n_{k2}=2$, $n_{k3}=1$. The model is estimated using the prediction error method; the degree of the model selection is carried out with the best AIC criterion (the structure that minimizes AIC).	FIT: 68.12%, FIT1: 63.02% FIT10: 58.29%, V: 0.138 FPE: 1.52, NSSE: 0.047
Black-box BJ model with $n_{b1}=1$, $n_{b2}=3$, $n_{b3}=1$, $n_c=3$, $n_d=2$, $n_f=2$, $n_{k1}=1$, $n_{k2}=3$, $n_{k3}=1$. The model is estimated using the prediction error method; the degree of the model selection is carried out with the best AIC criterion (the structure that minimizes AIC).	FIT: 100%, FIT1: 100% FIT10: 100%, V: 0.0237 FPE: 0.45, NSSE: 1.96e-20

Table 7. Milling of aluminium components. Function and parameters that represent the behaviour of the laser-milled piece for the angle error. The degree of the BJ model polynomials are $n_{b1}=3$, $n_{b2}=1$, $n_{b3}=1$, $n_c=3$, $n_d=2$, $n_f=2$, $n_{k1}=2$, $n_{k2}=1$, $n_{k3}=1$. [3 1 1 3 2 2 2 1 1].

Parameters and polynomials.	
$B_1(q) = -0.00552\ q^{-2} - 0.006068\ q^{-3} - 0.003629\ q^{-4}$	$D(q) = 1 - 1.804\ q^{-1} + 0.9627\ q^{-2}$
$B2(q) = -0.0001954\ q^{-1}$	$F1(q) = 1 + 0.4775\ q^{-1} + 0.1816\ q^{-2}$
$B3(q) = 0.004336\ q^{-1}$	$F2(q) = 1 - 0.4527\ q^{-1} + 0.8147\ q^{-2}$
$C(q) = 1 - 1.553\ q^{-1} + 0.555\ q^{-2} + 0.262\ q^{-3}$	$F3(q) = 1 - 0.554\ q^{-1} + 0.0992\ q^{-2}$ *e(t) is white noise signal with variance 0.78*

Table 8. Milling of aluminium components. Function and parameters that represent the behaviour of the laser-milled piece for the depth error. The degree of the BJ model polynomials are $n_{b1}=1$, $n_{b2}=3$, $n_{b3}=1$,$n_c=3$, $n_d=2$, $n_f=2$, $n_{k1}=1$, $n_{k2}=3$, $n_{k3}=1$. [1 3 1 3 2 2 1 3 1].

Parameters and polynomials.	
$B1(q) = = -0.00909\ q^{-1}$	$D(q) = 1 - 0.2621\ q^{-1} - 0.7457\ q^{-2}$
$B2(q) = 0.001451\ q^{-3} - 0.001019\ q^{-4} - 0.0001008\ q^{-5}$	$F1(q) = 1 - 0.3072\ q^{-1} + 0.7465\ q^{-2}$
$B3(q) = -0.01077\ q^{-1}$	$F2(q) = 1 - 0.1005\ q^{-1} + 0.5109\ q^{-2}$
$C(q) = 1 + 0.243\ q^{-1} + 0.7044\ q^{-2} - 0.4622\ q^{-3}$	$F3(q) = 1 + 0.9133\ q^{-1} + 0.53\ q^{-2}$ *e(t) is white noise signal with variance 0.23*

Table 9. Milling hardened steel components. Indicator values for several proposed models of the angle error.

Model	Performance Indexes
Black-box OE model with $n_{b1}=2$, $n_{b2}=1$, $n_{b3}=1$, $n_f=2$, $n_{k1}=1$, $n_{k2}=1$, $n_{k3}=1$. The model is estimated using the prediction error method; the degree of the model selection is carried out from the best AIC criterion (the structure that minimizes AIC).	FIT: 44.04%, FIT1: 44.04% FIT10: 44.04%, V: 0.02 FPE: 0.23, NSSE: 7.71e-4
Black-box OE model $n_{b1}=1$, $n_{b2}=1$, $n_{b3}=1$, $n_f=2$, $n_{k1}=1$, $n_{k2}=1$, $n_{k3}=1$. The model is estimated using the prediction error method; the degree of the model selection is carried out with the best AIC criterion (the structure that minimizes AIC).	FIT: 21.2%, FIT1: 21.2% FIT10: 21.2%, V: 0.023 FPE: 0.162, NSSE: 0.0015
Black-box BJ model with $n_{b1}=1$, $n_{b2}=1$, $n_{b3}=1$, $n_c=2$, $n_d=2$, $n_f=2$, $n_{k1}=1$, $n_{k2}=1$, $n_{k3}=1$. The model is estimated using the prediction error method; the degree of the model selection is carried out with the best AIC criterion (the structure that minimizes AIC).	FIT: 100%, FIT1: 100% FIT10: 100%, V: 0.12 FPE: 0.27, NSSE: 2.73e-31
Black-box BJ model with $n_{b1}=2$, $n_{b2}=1$, $n_{b3}=1$, $n_c=2$, $n_d=2$, $n_f=2$, $n_{k1}=1$, $n_{k2}=1$, $n_{k3}=1$. The model is estimated using the prediction error method; the degree of the model selection is carried out with the best AIC criterion (the structure that minimizes AIC).	FIT: 100%, FIT1: 100% FIT10: 100%, V: 0.97 FPE: 1,75, NSSE: 4.17e-30

Table 10. Milling hardened steel components. Indicator values for several proposed models of the depth error.

Model	Performance Indexes
Black-box OE model with $n_{b1}=1$, $n_{b2}=2$, $n_{b3}=1$, $n_f=2$, $n_{k1}=1$, $n_{k2}=2$, $n_{k3}=1$. The model is estimated using the prediction error method; the degree of the model selection is carried out from the best AIC criterion (the structure that minimizes AIC).	FIT: 100%, FIT1: 100% FIT10: 100%, V: 0.051 FPE: 0.636, NSSE: 1.08e-27
Black-box BJ model with $n_{b1}=1$, $n_{b2}=3$, $n_{b3}=1$, $n_c=2$, $n_d=1$, $n_f=1$, $n_{k1}=1$, $n_{k2}=2$, $n_{k3}=1$. The model is estimated using the prediction error method; the degree of the model selection is carried out with the best AIC criterion (the structure that minimizes AIC).	FIT: 100%, FIT1: 100% FIT10: 100%, V: 0.07 FPE: 1.331, NSSE: 1.24e-28
Black-box BJ model with $n_{b1}=2$, $n_{b2}=2$, $n_{b3}=2$, $n_c=2$, $n_d=1$, $n_f=1$, $n_{k1}=2$, $n_{k2}=2$, $n_{k3}=1$. The model is estimated using the prediction error method; the degree of the model selection is carried out with the best AIC criterion (the structure that minimizes AIC).	FIT: 65.16%, FIT1: 59.98% FIT10: 63.32%, V: -0.12 FPE:0.471, NSSE:0.0014

Table 11. Milling hardened steel components. Function and parameters that represent the behaviour of the laser-milled piece for the angle error. The degree of the BJ model polynomials are $n_{b1}=1$, $n_{b2}=1$, $n_{b3}=1$,$n_c=2$, $n_d=2$, $n_f=2$, $n_{k1}=1$, $n_{k2}=1$, $n_{k3}=1$. [1 1 1 2 2 2 1 1 1].

Parameters and polynomials.	
$B1(q) = 0.01269\ q^{-1}$	$D(q) = 1 + 1.208\ q^{-1} + 0.3098\ q^{-2}$
$B2(q) = 0.0004895\ q^{-1}$	$F1(q) = 1 + 0.4094\ q^{-1} - 0.16\ q^{-2}$
$B3(q) = 0.01366\ q^{-1}$	$F2(q) = 1 - 1.678\ q^{-1} + 0.7838\ q^{-2}$
$C(q) = 1 + 1.541\ q^{-1} + 1.02\ q^{-2}$	$F3(q) = 1 - 1.1\ q^{-1} + 0.7671\ q^{-2}$ *e(t) is white noise signal with variance 0.08*

Table 12. Milling hardened steel components. Function and parameters that represent the behaviour of the laser-milled piece for the depth error of the test piece. The degree of the OE model polynomials are $n_{b1}=1$, $n_{b2}=2$, $n_{b3}=1$,$n_f=2$, $n_{k1}=1$, $n_{k2}=2$, $n_{k3}=1$. [1 2 1 2 1 2 1].

Parameters and polynomials.	
$B1(q) = 0.003554\ q^{-1}$	$F1(q) = 1 - 0.4365\ q^{-1} - 0.1936\ q^{-2}$
$B2(q) = -0.00224\ q^{-2} - 0.003145\ q^{-3}$	$F2(q) = 1 - 0.5375\ q^{-1} - 0.4496\ q^{-2}$
$B3(q) = -0.02758\ q^{-1}$	$F3(q) = 1 - 1.677\ q^{-1} + 0.9613\ q^{-2}$ *e(t) is white noise signal with variance 0.34*